Molecular dynamics simulations of the initial stages of spall in nanocrystalline copper

Vladimir Dremov, Alexander Petrovtsev, Philipp Sapozhnikov, and Maria Smirnova
Russian Federal Nuclear Center, Institute of Technical Physics, Snezhinsk, 456770 Chelyabinsk reg., Russia

Dean L. Preston* and Marvin A. Zocher
Los Alamos National Laboratory, Los Alamos, New Mexico 87545, USA
(Received 23 January 2006; revised manuscript received 16 June 2006; published 30 October 2006)

Molecular dynamics simulations of the initial stages of the spall process in single nanocrystals and polynanocrystals of copper are performed. The simulations show that void nucleation in copper polynanocrystals occurs predominantly along the grain boundaries, whereas voids are formed at stacking fault intersections in copper monocrystals. The calculated spall strengths of single-crystal copper at strain rates of $2-4 \times 10^9$ s^{-1} are consistent with existing experimental data, and the polynanocrystal spall strength is found to increase rapidly at rates around 10^9 s^{-1} up to the theoretical ultimate spall strength of 22.5 GPa at about 3×10^9 s^{-1}.

DOI: 10.1103/PhysRevB.74.144110 PACS number(s): 62.50.+p, 02.70.Ns

I. INTRODUCTION

Molecular dynamics (MD) is a powerful technique for calculating the static and dynamic properties of materials. In this paper we report the results of MD simulations of the nucleation and early growth of material damage in single-nanocrystal and polynanocrystalline copper under dynamic tensile loading.

MD simulations of spall were first carried out for two-dimensional solids.[1] This pioneering work was followed by an investigation of damage formation in polycrystalline copper under high-rate volumetric strain using an EAM (embedded atom method) potential.[2] The volumetric strain rates were 10^8-10^{10} s^{-1} in systems ranging from 10^5 to 10^6 atoms. It was shown that vacancy interactions lead to the nucleation and growth of near-spherical voids in the bulk of the material and that the grain boundaries also serve as nucleation sites. In Ref. 3 an accurate many-body potential was used to study spall in Ta induced by high-velocity impact. Despite the rather small system size ($\sim 10^4$ particles $= 30 \times 16 \times 16$ unit cells) the void size distribution was obtained as a function of time. The most notable finding was that catastrophic failure coincides with a critical behavior characterized by a void distribution of the form $N(V) \sim V^{-G}$, where $G=2.2$, N is the number of voids, and V is the void volume.

In the present work we simulate the high-velocity impact of two samples of the same material, namely copper. The samples are rectangular parallelepipeds with equal square cross sections but differing thicknesses. The normals to the square sample faces are parallel to the relative velocity; these faces coincide upon impact. Periodic boundary conditions are used in the directions transverse to the relative velocity, while free boundary conditions are used in the longitudinal direction. Shock waves propagate away from the plane of impact, and later reflect from the back free surfaces of the samples as release waves. Superposition of the release waves in the longer sample results in the formation of a region of sufficient negative pressure (tension) to nucleate and grow voids that ultimately lead to spall (fracture) of the sample.

Experimental investigations of spall are typically carried out in planar geometries because of the relative simplicity of shock generation, diagnostics, and interpretation of results. Planar shock waves can be generated in a planar target by high explosives (HE), by high-power laser pulses, or by the impact of a plate or foil (typically propelled from a gas gun or by laser pulses). Since the focus of the present work is the simulation of high-velocity impact, let us consider this method,[4] and the physical processes that take place within the specimen during such an event. Upon impact, two compressive shock waves are generated, traveling in opposite directions from the plane of impact (the interface between impactor and target). When these shock waves reach the free surfaces of impactor and target, they reflect as rarefaction (release) waves, now traveling toward one another. Because the target is given a thickness twice that of the impactor, the rarefaction waves will converge at approximately the midplane of the target. The superposition of the two release waves results in a tensile pulse. If the magnitude of the tensile pulse exceeds a critical value (the spall strength of the material), spall fracture will occur.

The wave interactions just described are essentially the same as those that take place in our MD simulations. One difference between the MD simulation and the physical experiment that the simulation is designed to model is the use of periodic boundary conditions on the transverse surfaces (these are free surfaces in the physical experiment). This difference is physically unimportant since the plates used in an actual experiment are of sufficient diameter that the release waves from the transverse free surfaces traverse only a small portion of the sample on the time scale of the experiment. This means that the inner portion of the sample (the region where diagnostics are applied) experiences no effect from the transverse free surfaces and is exposed to a stress history that is well modeled by our simulation.

The impact velocities, and therefore peak stresses, in our MD simulations are comparable to those attained in an actual physical experiment, whether the drive is by gas gun or laser pulse. However, the small MD target thicknesses, $\sim 10^{-2}$ μm, lead to two significant differences between our simulations and experiment. First, the MD strain rates are around 10^9 s^{-1}, much higher than the rates typical of gas gun experiments, namely 10^5-10^6 s^{-1}. Second, the width of the

spall/damage zone roughly scales with sample thickness, hence the widths of the damage zones differ by 3–5 orders of magnitude.

We now discuss our MD simulations of the initial stages of spall in single-nanocrystal copper under loading along different crystallographic directions, as well as spall in polynanocrystals of copper.

II. MD SIMULATIONS OF SPALL IN SINGLE NANOCRYSTALS AND POLYNANOCRYSTALS

Calculations were carried out for monocrystalline copper samples with thicknesses of 66 and 144 unit cells and cross sections of 100×100 unit cells. Impact occurred at relative velocities of 1500, 2000, and 2500 m s^{-1} along the [100] crystallographic direction. The corresponding strain rates, which were obtained from the longitudinal velocity profiles, are estimated to be 2.25×10^9, 3.0×10^9, and 3.75×10^9 s^{-1}. A calculation was also carried out for an impact velocity of 2000 m s^{-1} along the [112] crystallographic direction. The shock wave pressures were sufficient in all cases to completely spall the samples. An EAM potential[5] was used for these simulations. The initial temperature was 300 K. Temperature control was not used in these nonequilibrium simulations.

Evolution of the longitudinal stress profile at an impact velocity of 2000 m s^{-1} for [100] loading is presented in Fig. 1. The resulting shock wave pressure is approximately 48 GPa, and the strain rate is about 3×10^9 s^{-1}. The region of elastic compression (elastic precursor) is only 5–10 unit cells wide, and it is of course followed by a plastic wave. Shear stress relaxation in such a strong shock wave in copper occurs through the formation of numerous stacking faults.[6] Elastic unloading, which is again followed by plastic flow, is discernible in Fig. 1 as a rapid drop in pressure to the left of the high-pressure plateaus at $t=9$ ps and $t=10.5$ ps. One can also see that overlap of the two rarefaction waves generates a high tensile stress, about 21 GPa, at 15 ps (see Fig. 1). The accompanying void formation (see below) implies that this stress is approximately equal to the spall strength. The spall process is evident in the longitudinal stress profiles for $t=16.5-19.5$ ps as the formation of a region of zero stress between regions of tensile stress.

Our estimated spall strength, 21 GPa, is close to the theoretical ultimate spall strength.[7] Using the experimental fit $D(U)=3.91+1.51U$ for copper,[8] where D is the shock wave velocity and U is the particle velocity, each in km s^{-1}, one constructs the Hugoniot $P(U)=\varrho_0 DU$, which has a minimum at $U_{\min}=-1.29$ km s^{-1}. Since the Hugoniot and the isentrope are second-order tangent to one another at the point $(\rho=\rho_0, U=0)$, the approximate spall strength for isentropic release, the theoretical ultimate spall strength, is $-P(U_{\min})=22.5$ GPa for copper.

In this paper we employ common neighbor analysis (CNA)[9] to determine the crystal structure and identify crystalline defects.

A calculated longitudinal section at $t=18$ ps for an impact velocity of 2000 m s^{-1} is presented in Fig. 2. Note that this figure, as well as Figs. 3 (right-hand side), 5, and 6 (right-hand side), show both the sample/target (144 unit cells thick, to the right) and the impactor (66 unit cells thick, to the left) in contact; in Figs. 3 (right-hand side) and 6 (right-hand side), nearly all of the impactor is covered by the experimental photomicrograph to the left. Figure 2(a) shows numerous voids with diameters of 5–8 unit cells localized in a developing spall plane. The initial stage of void formation is shown in Fig. 2(b). In the left-hand picture, the high tensile stress has formed an incipient rectangular void with a width of about one unit cell. During the next 0.2 ps, vortical atomic motion around the embryonic nanovoid gives it a spherical conformation, as shown on the right-hand picture. Thus the initial stage of spall in copper is the nucleation of spherical voids, even though the macroscopic tensile stress field is one dimensional. The growing void rapidly increases its surface area as new surface atoms emerge from the bulk of the sample. This high-rate process leads to amorphization of the material in the vicinity of the void, which in turn allows the void to retain a spherical shape as it grows. MD simulations of spall in CuTi alloy likewise show voids surrounded by

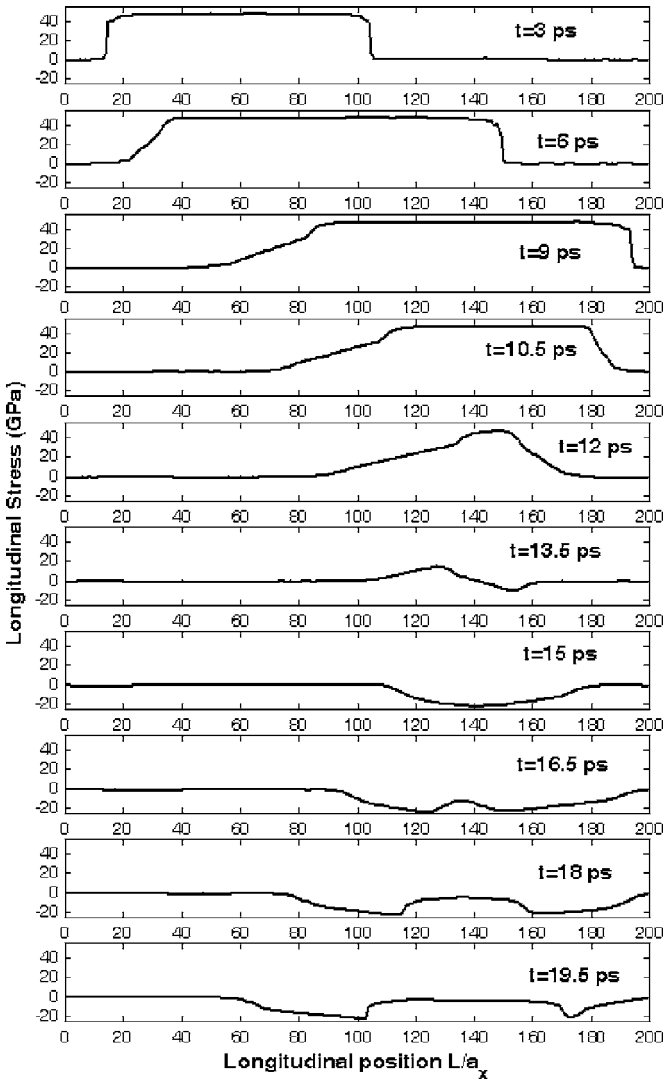

FIG. 1. Evolution of the longitudinal stress profile for a 48 GPa shock (2000 m s^{-1} impact velocity) propagating in the [100] direction.

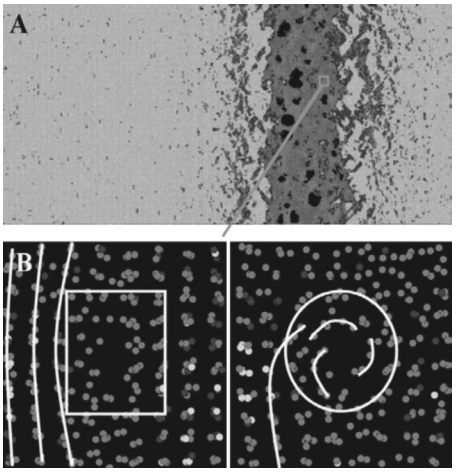

FIG. 2. (a) Longitudinal section (200×100 unit cells) of the copper single nanocrystal (2000 m s^{-1} impact velocity) at $t=18$ ps. The light gray coloring indicates the undamaged fcc lattice, while dark gray corresponds to amorphous regions. (b) Initial stage of void formation.

amorphous regions.[10] Our simulations also show that, prior to void coalescence, the region around the spall plane in a copper single nanocrystal is amorphous. We note, however, that spall planes in recovered samples (see, e.g., the photomicrograph of a recovered single-crystal copper sample in Fig. 3) may not be amorphous because of recrystallization, which occurs on a time scale much greater than that of our MD simulations, namely 30–50 ps. To date there have been no measurements of the material structure (crystalline versus amorphous) along the spall planes of recovered samples.

We calculated the stress distribution over the spall plane just before nucleation of the first voids. We found that the stress fluctuations over the plane were less than 1 GPa. Thus a void nucleates at a given point not because of a significantly larger stress but because the atomic configuration in the vicinity of that point is such that the local strength is relatively low.

Figure 3 is a qualitative comparison of our calculated longitudinal section at 20 ps to experiment. The left-hand picture is a photomicrograph of an incomplete spall plane (region of high void density) in a soft-recovered single-crystal

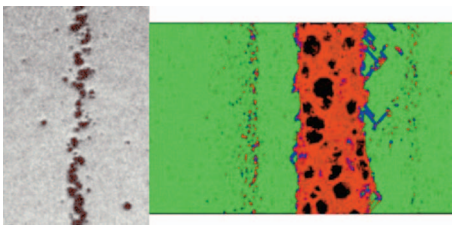

FIG. 3. (Color) (Left-hand side) Photomicrograph of a single-crystal copper sample from a soft recovery experiment;[11] the damaged region is roughly 40 μm wide. (Right-hand side) Longitudinal section (150×100 unit cells) of the simulated damage plane at $t=20$ ps in the monocrystalline copper sample loaded to 48 GPa in the [100] direction. Green corresponds to the initial fcc structure, while red and blue correspond to regions of undefined structure and stacking faults respectively.

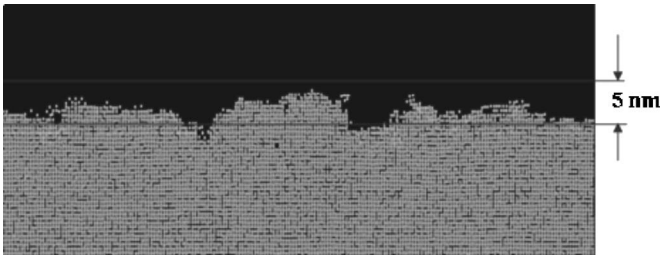

FIG. 4. Roughness of the spall surface (2000 m s^{-1} impact velocity) for [100] loading.

copper sample.[11] The damaged region is approximately 40 μm wide, and the characterisitic void diameter is ~10 μm. The microstructure of the material in the vicinity of the voids was not measured. In contrast, the incomplete spall plane in our MD simulation at 20 ps has a thickness of about 40 unit cells $\sim 10^{-2}$ μm, and the characteristic void diameter is ~3–5 nm. Despite the vast difference in length scales, the experimental and MD results are qualitatively similar.

As mentioned above, the 48 GPa shock pressure is sufficient to completely spall the sample. We estimate the roughness of the spall surface to be 5 nm as depicted in Fig. 4.

MD simulations of spall in copper single crystals were also carried out for [100] loading at impact velocities of 1500 and 2500 m s^{-1}. At 1500 m s^{-1} the strain rate, $\dot{\epsilon}$, is approximately 2.25×10^{9} s^{-1}, and the spall strength, σ_s, is 21.0 GPa. The strain rate at 2500 m s^{-1} is larger than that at 1500 m s^{-1} by a factor of 5/3, i.e., $\dot{\epsilon}=3.75\times10^{9}$ s^{-1}, but the spall strength is essentially unchanged: $\sigma_s=21.3$ GPa.

An MD simulation was carried out for loading along the crystallographic direction [112] at a single impact velocity, namely 2000 m s^{-1}. Figure 5 illustrates the microstructural changes taking place in the sample under shock loading and subsequent release. Because of the asymmetric orientation of the crystal lattice relative to the shock front, stacking faults are formed with a preferred orientation [mostly (111) and $(\bar{1}11)$ slip planes are activated]. Void formation begins in bands (contoured in Fig. 5) having the same orientation as the stacking faults. These bands are separated by narrow regions of relatively undisturbed material (light gray "islands" between the void bands) which later become freely moving fragments that are not observed in the case of [100] shock loading.

It is difficult to estimate the roughness of the spall surface but it is much greater than in the case of [100] loading.

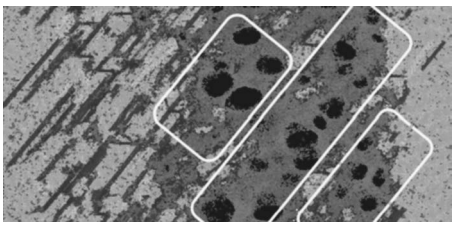

FIG. 5. Longitudinal section (200×100 unit cells) of the single-crystal copper sample strained in the [112] direction (2000 m s^{-1} impact velocity). Light gray corresponds to the fcc structure, and dark gray indicates amorphous regions.

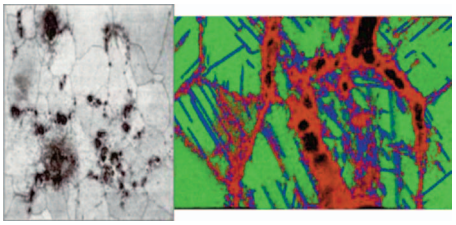

FIG. 6. (Color) (Left-hand side) Photomicrograph (40 μm wide) of a copper polycrystalline sample from a soft recovery experiment.[11] (Right-hand side) Longitudinal section (150×100 unit cells) of copper polynanocrystal at $t=20$ ps for a collision velocity of 2000 m s^{-1}. Green corresponds to the initial fcc structure, while red and blue correspond to regions of structural defects including grain boundaries and stacking faults.

Polycrystalline samples for our MD simulations were constructed by filling Voronoi cells with randomly oriented single crystals with a common lattice constant corresponding to an elevated pressure of order 2 GPa. Relaxation of the samples (relaxation time was 60 ps) at the elevated pressure and $T=300$ K ensured that the grains were contiguous. After relaxation, the samples were rescaled to ambient density. The characteristic grain size was ~20 nm.

The polycrystal simulations were carried out for three impact velocities, namely 1500, 2000, and 2500 m s^{-1} with corresponding strain rates of 2.25×10^9, 3.0×10^9, and 3.75×10^9 s^{-1}. The spall strengths at these impact velocites (strain rates) proved to be 15.0, 20.0, and 20.1 GPa, respectively. Here it should be noted that σ_s rises rapidly from 15 GPa at 2.25×10^9 s^{-1} to nearly the theoretical ultimate spall strength, 22.5 GPa, at 3.0×10^9 s^{-1}.

Incipient spall in copper polynanocrystals (see Fig. 6) involves the formation of spherical voids, just as in single nanocrystals. Although numerous stacking faults are formed in the bulk of the grains as a result of shear stress relaxation (see also Ref. 12 for shear stress relaxation in nanomaterials), the voids are concentrated at the grain boundaries: at a collision velocity of 1500 m s^{-1} there are no voids produced in the bulk of the grains, but at higher impact velocities some voids are formed in the grain interiors.

In contrast to Fig. 3, which is a qualitative comparison of one of our simulations to experiment, Fig. 7 is a quantitative comparison of simulated and experimental void densities through the spall plane. Since the distance from the spall plane is normalized by the sample thickness, it is clear from the figure that the width of the material damage zone approximately scales with the sample thickness. Note that the polycrystal void distributions are irregular and asymmetric around the spall planes, and that the asymmetry for x/L within roughly one-tenth unit of the spall plane is greater for the simulated distribution than for the experimental one. This is because the ratio of the grain size to the width of the damage zone is greater in the MD simulations.

In Fig. 8 we plot the spall strength of both polycrystalline and single-crystal copper as a function of strain rate. For $\dot{\epsilon}<10^8$ s^{-1}, the polycrystal spall strengths determined from macroscopic shock-wave experiments,[13,14] ($\otimes$) and laser-driven miniflyers[15] ($\oplus$) are fit very accurately by the power law $\sigma_s=0.14\dot{\epsilon}^{1/5}$ GPa ($\log_{10}\sigma_s=0.20\log_{10}\dot{\epsilon}-0.85$). The

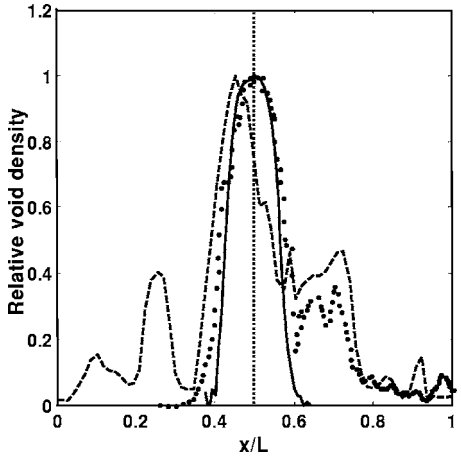

FIG. 7. Relative void density (ρ/ρ_{max}) versus distance normal to the spall plane; the through-plane coordinate x, whose origin is on the impact surface, is normalized by the specimen thickness, L. The points are 3D tomographic data from the soft recovered polycrystalline copper sample shown in Fig. 6 (left-hand side) [11] The dashed (solid) line shows MD results for a polycrystal (single-crystal) sample (2000 m s^{-1} impact velocity) just before void coalescence.

polynanocrystal data of Germann and Valone[16] ($\odot$) at $\dot{\epsilon}\approx10^{10}$ s^{-1} lie just 5% below this straight-line fit. The polynanocrystal spall strengths calculated here ($\times$) lie 15%–25% above the straight-line fit, and suggest that the polycrystal spall strength departs from the $\dot{\epsilon}^{1/5}$ behavior at $\dot{\epsilon}\approx10^9$ s^{-1} and then rapidly increases to the ultimate spall strength[7] at $\dot{\epsilon}\approx3\times10^9$ s^{-1}; the spall strength at higher rates

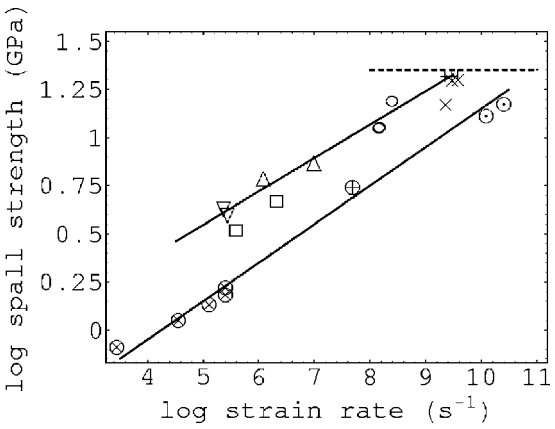

FIG. 8. Spall strength (σ_s) as a function of strain rate ($\dot{\epsilon}$); the logarithms are both base 10. The triangles are experimental results for [100] loading of single crystals by Razorenov and Kanel[14] ($\bigtriangledown$) and Tonks *et al.*[17] ($\bigtriangleup$). The linear least squares fit to these data is $\log_{10}\sigma_s=0.17\log_{10}\dot{\epsilon}-0.27$, which is the upper line in the figure. Our MD results for [100] loading (+) lie near the intersection of this fit with the horizontal dashed line at 22.5 GPa ($\log_{10}\sigma_s=1.35$), the theoretical ultimate spall strength.[7] The squares are data for [111] loading.[14] The polycrystal data include our MD results ($\times$), the MD data of Germann and Valone[16] ($\odot$), the experimental data of Kanel *et al.*[13] and Razorenov and Kanel[14] ($\otimes$), and the laser-driven miniflyer data of Paisley *et al.*[15] ($\oplus$). The least squares fit to the experimental polycrystal data, $\log_{10}\sigma_s=0.20\log_{10}\dot{\epsilon}-0.85$, is the lower line in the figure. The open circles are the data of Moshe *et al.*[18]

is expected to equal the ultimate spall strength.

Three sets of experimental single-crystal spall strength data are included in Fig. 8. The single-crystal spall strength for shock propagation in the [111] direction (squares) increases with $\dot{\epsilon}$ at the same rate as observed in polycrystals, at least for $\dot{\epsilon} < 10^8$ s^{-1}. The least squares fit to the data for [100] loading from Razorenov and Kanel[14] (∇) and Tonks *et al.*[17] ($\triangle$) is given by $\log_{10} \sigma_s = 0.166 \log_{10} \dot{\epsilon} - 0.274$. The results of the present work (+) deviate from this line by at most 3%, and lie within 1.5 GPa of the theoretical ultimate spall strength of 22.5 GPa. As for polycrystals, the single-crystal spall strength at rates exceeding about 3×10^9 s^{-1}is expected to equal the ultimate spall strength.

Finally, we mention the high-rate spall strength data of Moshe *et al.*[18] obtained by laser-induced shock loading of thin (1–10 μm) copper foils; their three data points are shown as open circles in Fig. 8. Unfortunately, the mean grain size in their copper foils is not quoted, so we do not know if their results should be interpreted as single-crystal or polycrystal data, or neither, if the grain size is of order the foil thickness. Here we only note that their data differ from the single-crystal straight line fit by at most 5%, and the data are not consistent with the MD results for polycrystals included in Fig. 8.

III. CONCLUDING REMARKS

A series of molecular dynamics simulations was carried out to investigate the initial stages of spallation in single nanocrystals and polynanocrystals of copper. It was found that the microstructures of the developing spall planes in monocrystals are strongly dependent on the direction of shock loading relative to the lattice orientation. Void nucleation in copper polynanocrystals occurs predominately along the grain boundaries, whereas voids are formed at stacking fault intersections in copper monocrystals. Nevertheless, the spall strength of the polynanocrystal is identical to that of single-nanocrystal copper at strain rates above approximately 3×10^9 s^{-1}.

Our MD simulations provide numerical data on microscale damage and failure mechanisms taking place on a time scale of order 10 ps and spatial scales up to 100 nm. Processes occurring over longer temporal and larger spatial scales, such as recrystallization and mesoscale void growth, are inaccessible to MD simulations. The strain rates in our simulations are very high, about 10^9 s^{-1}, whereas the strain rate in a cm-sized sample at the same level of loading considered in our MD calculations is approximately five orders of magnitude smaller. Nevertheless, MD simulations play a vital role in multiscale modeling of material damage and failure: they provide early-time microscale data on nucleation mechanisms in both single crystals and polycrystals as well as spall strengths at very high strain rates, which are unavailable experimentally.

ACKNOWLEDGMENTS

The work was performed under Contract No. 04783-000-99-35 between the Institute of Technical Physics and Los Alamos National Laboratory.

*Electronic address: dean@lanl.gov

[1] N. J. Wagner, B. L. Holian, and A. F. Voter, Phys. Rev. A **45**, 8457 (1992).
[2] J. Belak, *AIP Conference Proceedings* (AIP, New York, 1998), Vol. 429, p. 211.
[3] A. Strachan, T. Çağın, and W. A. Goddard III, Phys. Rev. B **63**, 060103(R) (2001).
[4] D. Grady and M. Kipp, "Dynamic fracture and fragmentation," in *High-Pressure Shock Compression of Solids*, edited by J. Asay and M. Shahinpoor (Springer-Verlag, New York, 1993), Chap. 8.
[5] R. A. Johnson, Phys. Rev. B **37**, 3924 (1988).
[6] B. Holian and P. Lomdahl, Science **280**, 2085 (1998).
[7] G. Kanel, S. Razorenov, A. Utkin, and V. Fortov, *Shock Wave Phenomena in Condensed Matter* (Yanus-K, Moscow, 1996).
[8] *LASL Shock Hugoniot Data*, edited by S. Marsh (University of California Press, Berkeley, Los Angeles, London, 1980).
[9] J. Honeycutt and H. Andersen, J. Phys. Chem. **91**, 4950 (1987).
[10] Y. Ashkenazy and R. Averbach, Appl. Phys. Lett. **86**, 051907 (2005).
[11] K. Budil, J. Belak, R. Becker, G. Campbell, F. Garaizar, D. Kalantar, and D. Nikkel, LLNL Report No. UCRL-PRES-149124. See also http://www.llnl.gov/str/
[12] F. Sapozhnikov, V. Dremov, and M. Smirnova, J. Phys. IV **110**, 323 (2003).
[13] G. Kanel, S. Razorenov, and V. Fortov, Sov. Phys. Dokl. **29**, 241 (1984).
[14] S. Razorenov and G. Kanel, Phys. Met. Metallogr. **74**, 526 (1992).
[15] D. Paisley, R. Warnes, and R. Kopp, "Laser-driven flat plate impacts to 100 GPa with subnanosecond pulse duration and resolution for material property studies," in *Shock Compression of Condensed Matter 1991*, edited by S. C. Schmidt, R. D. Dick, J. W. Forbes, and D. G. Tasker (Elsevier, New York, 1992), p. 825.
[16] T. Germann and S. Valone, Report No. LA-UR-05-7623.
[17] D. Tonks, D. Alexander, S. Sheffield, D. Robbins, A. Zurek, and W. Thissell, J. Phys. IV **10**, (2000).
[18] E. Moshe, S. Eliezer, Z. Henis, M. Werdiger, E. Dekel, Y. Horovitz, S. Maman, I. Goldberg, and D. Eliezer, Appl. Phys. Lett. **76**, 1555 (2000).